Effect of axial deformation on flutter of cantilevered FGM cylindrical shells under axial follower forces

M.E. Torki[1], M. Taghi Kazemi[2], S.B. Talaeitaba[3]*

Abstract

The effect of axial deformation of shell particles on the dynamic instability (flutter) of cantilevered cylindrical shells made of functionally graded materials (FGM) under an end axial follower force is addressed. To this end, at first, results for free vibration of FGM cylindrical shells were verified with previous outcomes and they were in very good agreement. Then, the effect of axial deformation of the shell, acting like a reducing linearly-distributed follower load, on the critical circumferential mode number and the flutter load of FGM shells was accounted for. Finally, the effect of axial deformation of the shell particles on the critical circumferential mode number and the flutter load of FGM shells were investigated. In this case, three homogeneous shells with different elasticity moduli and densities and two FGM materials were considered: nickel-stainless steel and stainless steel-alumina. Results include the increasing critical circumferential mode number and the increasing value of the flutter load due to axial deformation. The increase in the flutter load occurs in proportion to the whole elasticity modulus of the material, and thus it can be derived from the formula of mixture for an FGM.

Keywords: Flutter, Follower force, Functionally graded material (FGM), Power parameter, Axial deformation.

1. Introduction

In recent years, *Functionally-Graded Materials* (*FGM*) have received wide applications in engineering mechanics since laminated composites can encounter delamination when undergoing great mechanical or temperature loads due to different deformation fields occurring in different layers which lead to inter-layer stresses. Thus, in order to control the mechanical properties including the amounts and localities of temperature stresses, yielding and ultimate strengths, and crack stimuli and zones, *FGM* materials are generally preferable to laminated composites [1]. Of the most notable applications of *FGM* is in air-plane landing gears, reservoirs containing chemical, radioactive, or plasma settings, high-speed aircrafts (including skin structures such as fuselages), propulsion systems in air planes, cutting instruments, incinerators, heat exchangers, turbine blades, etc. [2-7].

A follower force is a non-conservative destabilizing force which changes direction in parallel to the rotation of its application point.

* *Corresponding author: talaeetaba@iaukhsh.ac.ir*

1 PhD student, Zachry Department of Civil Engineering, Texas A&M University, College Station, TX 77843, USA

2 Associate professor, Department of Civil Engineering, Sharif University of Technology, Tehran, Islamic Republic of Iran

3 Assistant Professor of Azad University, Department of Civil Engineering, Khomeinishahr Azad University, Isfahan, Islamic Republic of Iran

By its very nature, it mostly applies to axially loaded structures. Hence, the use of stiffening elements proves significantly effective in delaying instability (This will pose an interesting subject for future work in this respect since the effect of stiffening elements on flutter of FGM structures has not been reported as investigated) [8-10].

Flutter is known as dynamic instability occurring with infinite frequency of the structure body. The most well-known problem in flutter of cantilever structures is Beck's problem, in which a concentrated follower force is applied at the free end of a cantilever. Practical applications of this problem include the thrust applied on the end of a projectile or missile by a rocket, the thrust applied on the body of aircraft structures by a jet engine, gas turbine rotors, the gripping force in disk brakes, the eccentric load exerted on a platform by a tip mass, etc. [8-10].

Research works about flutter of *homogeneous* cylindrical shells under follower forces abound. Altman and De Oliviera studied the dynamic stability of cantilever cylindrical and conical panels with and without slight internal damping. They asserted that due to numerical defects, the critical load calculated becomes occasionally very small. To overcome this problem, a slight damping matrix proportional to the stiffness matrix can be used in the solution [11, 12]. Dynamic stability of thin cylindrical panels with different boundary conditions under concentrated and distributed follower forces was firstly studied by Bismark Nasr using the finite element method with C^l continuity [13]. The dynamic stability of free-free cylindrical shells under end follower forces was studied by

Park and Kim [14]. They used the finite element method with the First-order Shear Theory (*FST*) theory. They extracted the critical loads, critical sequential modes, and critical circumferential mode numbers for different length-to-radius (*L/R*) and thickness-to-radius (*h/R*) ratios. They concluded that *FST* is valid only for $L/R > 20$, and for $L/R > 40$ the cylindrical shell can be analyzed with the beam theory in certain regions of *h/R*. The same problem for cantilever cylindrical shells was studied by Torki et al. [15]. They modified the static part of the axial deformation of a free-free shell into that of a cantilever shell and verified the obtained flutter load for a cantilever shell with that of a long free-free shell, for which the results were in good agreement. They calculated the increased flutter load due to considering the effect of axial deformation for different values of *L/R* and *h/R* ratios.

Flutter of *FGM* materials has been studied by many researchers. Prakash and Ganapathi and Sohn and Kim studied the stability problem in plane panels, Navazi and Haddadpour studied the problem in plates, and Haddadpour et al. considered the problem in cylindrical shells, and Ebrahim et al. solved the problem in nonlinear regions for temperature loads [16, 17]. Haddadpour et al. studied flutter of *FGM* plates under supersonic air flows by using the Classic Plate Theory (*CST*) and considering the von Karman nonlinearity.

They used the Galerkin method with 6 longitudinal modes for convergence, and discovered that the maximum flutter threshold occurs due to a specific power parameter between zero and infinity [18]. Haddadpour et al. assessed the supersonic flutter problem of *FGM* cylindrical shells by using Love's hypotheses and the von Karman nonlinear effect to derive the differential equations and using the first Piston theory to calculate the follower force exerted by air.

They used the Galerkin method with polynomial mode shapes to solve the equation systems, and used a polynomial function for the temperature distribution along the thickness. They concluded that the effect of temperature is so rigorous that the flutter load declines to zero for some temperatures near the buckling temperature [19].

Although there is a large cache of work concerning the flutter of homogeneous cylindrical shells under follower forces, to the best of the authors' knowledge, it seems that work on the corresponding problem for *FGM* shells is meager. Thus, the dynamic stability of *FGM* cylindrical shells under follower forces will be discussed in the sequel. For this purpose, Love's hypotheses are used to derive the differential equations of motion, and the extended Galerkin method is used to solve the equation systems.

The problem is solved for three homogeneous (nickel, stainless steel, and alumina) and two *FGM* materials (nickel-stainless steel and stainless steel-alumina). Results include the effect of density and the power parameter on the critical circumferential mode number and the minimum flutter load, in the case of considering the axial deformation, in different ranges of the shell thickness and length.

2. Theoretical Formulation

2.1. Displacement field and strains

Consider a cylindrical shell with radius R, thickness h, and length L. In case that the coordinate system is taken to be as shown in Fig. 1a, then using FST, the deformation components of any point can be written as [20]:

$$u(x,\theta,z,t) = u_0(x,\theta,t) + z\,\phi_x(x,\theta,t)$$
$$v(x,\theta,z,t) = v_0(x,\theta,t) + z\,\phi_\theta(x,\theta,t) \qquad (1)$$
$$w(x,\theta,z,t) = w_0(x,\theta,t)$$

where u_0, v_0, and w_0 are the displacement components of the middle surface and ϕ_x and ϕ_θ are changes in the slope of the normal to the middle surface around θ and x axes, respectively. The strain resultants per unit length for a cylindrical shell are shown in Fig. (1b).

For the strain components, Love's hypotheses are used. These hypotheses express the following [20]:

The transverse normal is inextensible.

Normals to the reference surface of the shell before deformation remain straight, but not necessarily normal, after deformation.

Deflections and strains are infinitesimal.

The transverse normal stress is negligible (plane-stress state is invoked).

Using Eq. (1) and by considering Love's hypotheses expressed above, the strain tensor elements can be written as follows [20]:

$$\varepsilon_1 = \varepsilon_1^0 + z\,\varepsilon_1^1, \quad \varepsilon_2 = \frac{1}{1+z/R}\left(\varepsilon_2^0 + z\,\varepsilon_2^1\right)$$
$$\varepsilon_6 = \omega_1^0 + z\,\omega_1^1 + \frac{1}{1+z/R}\left(\omega_2^0 + z\,\omega_2^1\right) \qquad (2)$$
$$\varepsilon_4 = \frac{1}{1+z/R}\varepsilon_4^0, \quad \varepsilon_5 = \varepsilon_4$$

where the superscripted components are defined as:

$$\varepsilon_1^0 = \frac{\partial u_0}{\partial x}, \quad \varepsilon_2^0 = \frac{1}{R}\left(\frac{1}{R}\frac{\partial v_0}{\partial \theta} + \frac{\partial R}{\partial x}u_0 + w_0\right)$$
$$\varepsilon_4^0 = \frac{1}{R}\left(\frac{1}{R}\frac{\partial w_0}{\partial \theta} + R\phi_\theta - v_0\right), \quad \varepsilon_5^0 = \frac{\partial w_0}{\partial x} + \phi_x$$
$$\omega_1^0 = \frac{\partial v_0}{\partial x}, \quad \omega_2^0 = \frac{1}{R^2}\frac{\partial u_0}{\partial \theta} \qquad (3)$$
$$\varepsilon_1^1 = \frac{\partial \phi_x}{\partial x}, \quad \varepsilon_2^1 = \frac{1}{R^2}\frac{\partial \phi_\theta}{\partial \theta}$$
$$\omega_1^1 = \frac{\partial \phi_\theta}{\partial x}, \quad \omega_2^1 = \frac{1}{R^2}\frac{\partial \phi_x}{\partial \theta}$$

In a FGM material, the effective mechanical properties including elasticity modulus and Poisson's ratio, and physical parameters such as the density, thermal elongation coefficient, and thermal conductivity can be obtained using Eq. 4, known as the mixture law [21]:

$$F_{eff}(T,z) = F_m(T)V_m(z) + F_c(T)\left[1 - V_m(z)\right] = \left[F_m(T) - F_c(T)\right]V_m(z) + F_c(T), V_m = \left(\frac{z}{h} + \frac{1}{2}\right)^N, N \geq 0 \quad (4)$$
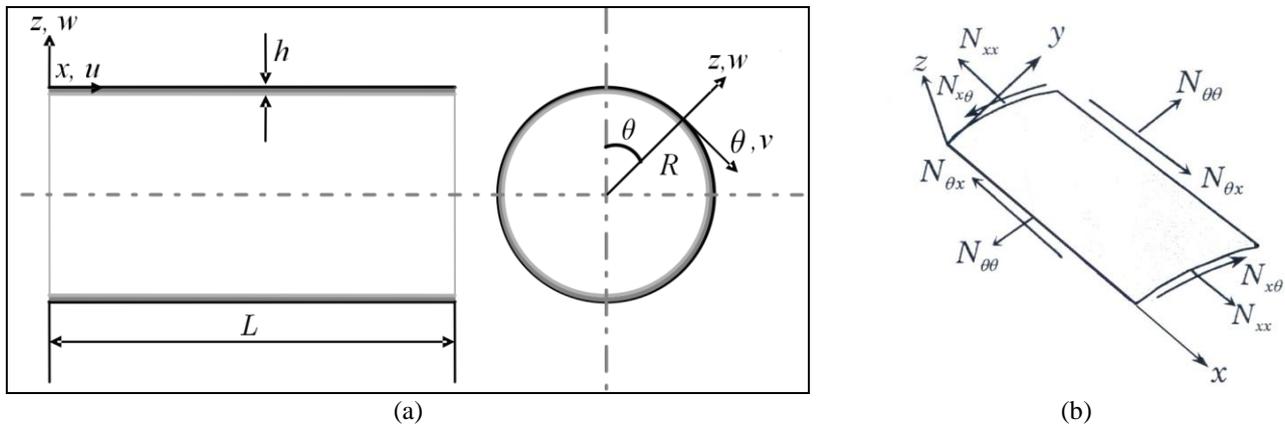

(a)   (b)

Fig. 1 (a) The coordinate system, (b) strain resultants considered for cylindrical shells [20]

where F_{eff} is the effective mechanical or physical property in the cross section, F_m and F_c are the corresponding parameters for the metal and ceramic phases, respectively, and V_i is the volume fraction, either for the metal (m) or ceramic (c) phase. The metal phase has greater elasticity modulus and lower density and Poisson's ratio, and the ceramic phase has less elasticity modulus and larger density and Poisson's ratio [24]. N, i.e. the power parameter, denotes the mathematical shape according to which the two phases change towards each other. When N equals unity, one phase approaches the other in a linear manner, and the effective property F_{eff} at the origin ($z = 0$) is the average of the corresponding properties for metal (F_m) and ceramic (F_c) phases. Figure 2 shows the outline of V_m against N. In the case the volume fraction is defined according to Eq. 4, the whole *FGM* elasticity modulus increases while its density decreases with N. In this case, the ceramic and metal phases are placed in the interior and exterior of the cross section, respectively, as depicted in Fig. 3.
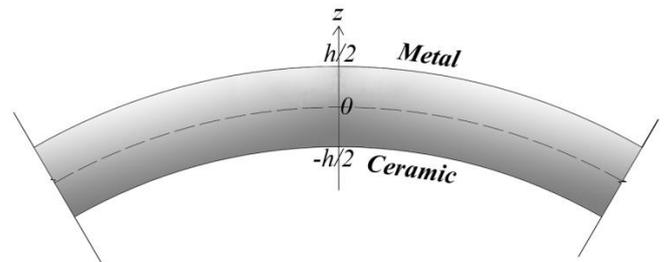

Fig. 3 *FGM* cylindrical section defined using Eq. 4.

The properties of FGM materials are temperature-dependent. Thus, the properties of each phase, including elasticity modulus, density, Poisson's ratio, etc. ought to be calculated in terms of temperature. Assuming that the so-called property is shown with F, the thermo-mechanical coupling effect of temperature T (by Kelvin) can be written as [21]:

$$F_i = F_0\left(F_{-1}T^{-1} + 1 + F_1T + F_2T^2 + F_3T^3\right)$$

$$F_i : E, \alpha, \kappa, \nu \text{ for metal and ceramic}$$

(5)

where the temperature coefficients can be obtained from Tables 1 and 2 for elasticity modulus and Poisson's ratio, respectively [21].

In the present research, the temperature has been assumed to be constantly equal to the base temperature, i.e. 300 K. In this case, the elasticity moduli of nickel, stainless steel, and alumina will be obtained 2.051×10^{11}, 2.07788×10^{11}, and 3.20235×10^{11} Pa, respectively and no extra stresses will be developed due to temperature change. Likewise, the Poisson's ratios of nickel, stainless steel, and alumina will be 0.31, 0.3176, and 0.26, respectively. Finally, according to the existent literature, the density of nickel, stainless steel, and alumina are 8900, 8166, and 4000 kg/m^3, respectively [22].
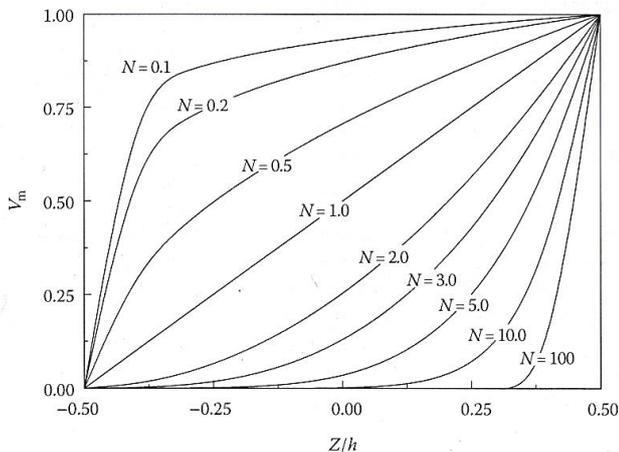
Fig. 2 Outline of V_m against the power parameter N.

Table 1 Temperature coefficients in Eq. 5 for elasticity modulus (*Pa*) [21]

Material	F_0	F_{-1}	F_1	F_2	F_3
Zirconia	244.27×10^9	0	-1.371×10^{-3}	1.214×10^{-6}	-3.681×10^{-10}
Alumina	349.55×10^9	0	-3.853×10^{-4}	4.027×10^{-7}	-1.673×10^{-10}
Silicon nitride	348.43×10^9	0	-3.070×10^{-4}	2.160×10^{-7}	-8.946×10^{-11}
$Ti-6Al-4V$	122.56×10^9	0	-4.586×10^{-4}	0	0
Stainless steel	201.04×10^9	0	3.079×10^{-4}	-6.534×10^{-7}	0
Nickel	223.95×10^9	0	-2.794×10^{-4}	-3.998×10^{-9}	0

Table 2 Temperature coefficients in Eq. 5 for Poisson's ratio [21]

Material	F_0	F_{-1}	F_1	F_2	F_3
Zirconia	0.288	0	1.133×10^{-4}	0	0
Alumina	0.260	0	0	0	0
Silicon nitride	0.240	0	0	0	0
$Ti-6Al-4V$	0.288	0	1.121×10^{-4}	0	0
Stainless steel	0.326	0	-2.002×10^{-4}	3.797×10^{-7}	0
Nickel	0.310	0	0	0	0

The stress resultant vectors in unit length (of the shell circumference), {N}, {M}, and {Q} for FGM can be obtained in terms of strain components using the ABD matrix as [20]:

$$
\begin{bmatrix} \{N\} \\ \{M\} \end{bmatrix} = \begin{bmatrix} [A] & [B] \\ [B] & [D] \end{bmatrix} \begin{bmatrix} \{\varepsilon^0\} \\ \{\varepsilon^1\} \end{bmatrix}, \quad \{\varepsilon^0\} = \begin{Bmatrix} \varepsilon_1^0 \\ \varepsilon_2^0 \\ \varepsilon_6^0 \end{Bmatrix}, \quad \{\varepsilon^1\} = \begin{Bmatrix} \varepsilon_1^1 \\ \varepsilon_2^1 \\ \varepsilon_6^1 \end{Bmatrix}, \quad \varepsilon_6^0 = \omega_1^0 + \omega_2^0, \quad \varepsilon_6^1 = \omega_1^1 + \omega_2^1
$$

$$
\begin{Bmatrix} Q_2 \\ Q_1 \end{Bmatrix} = K_s \begin{bmatrix} A_{44} & A_{45} \\ A_{45} & A_{55} \end{bmatrix} \begin{Bmatrix} \varepsilon_4^0 \\ \varepsilon_5^0 \end{Bmatrix}
\tag{6}
$$

where the components are defined as:

$$
\left(A_{ij}, B_{ij}, D_{ij}\right) = \int_{-h/2}^{h/2} S_{ij}(z)\left(1, z, z^2\right) dz, \quad (i, j = 1, 2, 6)
$$

$$
A_{ij} = \int_{-h/2}^{h/2} S_{ij}(z) dz, \quad (i, j = 4, 5)
\tag{7}
$$

$$
S_{11} = S_{22} = \frac{E(z)}{1-\upsilon^2(z)}, \quad S_{12} = S_{21} = \frac{\upsilon E(z)}{1-\upsilon^2(z)}, \quad S_{44} = S_{55} = S_{66} = \frac{E(z)}{2[1+\upsilon(z)]}
$$

where K_s is the shear correction factor, which is $\pi^2/12$ for cylindrical shells [2], and υ is Poisson's ratio. $E(z)$, $\rho(z)$, and $\upsilon(z)$ must be determined using Eq. 4 or 5. However, since the Poisson's ratios of the two phases are not far different, $\upsilon(z)$ can be taken equal for the two phases, i.e. constant for the whole thickness [23].

2.2. Equations of motion

In order to derive the governing equations of motion, Hamilton's principle is used as [20]:

$$
\int_0^T \left[\delta K - \delta U + \delta W_{nc}\right] dt = 0
\tag{8}
$$

where δK and δU are variations of kinetic energy and strain energy, respectively, defined as:

$$\delta K = \int\limits_0^L \int\limits_0^{2\pi} \Big[I_0 \big(\dot{u}_0 \delta \dot{u}_0 + \dot{v}_0 \delta \dot{v}_0 + \dot{w}_0 \delta \dot{w}_0 \big) + I_1 \big(\dot{\phi}_x \delta \dot{u}_0 + \dot{u}_0 \delta \dot{\phi}_x + \dot{\phi}_\theta \delta \dot{v}_0 + \dot{v}_0 \delta \dot{\phi}_\theta \big) + I_2 \big(\dot{\phi}_x \delta \dot{\phi}_x + \dot{\phi}_\theta \delta \dot{\phi}_\theta \big) \Big] R dx d\theta$$

$$\delta U = \int\limits_0^L \int\limits_0^{2\pi} \Big[N_x \delta \varepsilon_1^0 + M_x \delta \varepsilon_1^1 + N_\theta \delta \varepsilon_2^0 + M_\theta \delta \varepsilon_2^1 + \big(N_{x\theta} \delta \omega_1^0 + N_{\theta x} \delta \omega_2^0 \big) + \big(M_{x\theta} \delta \omega_1^1 + M_{\theta x} \delta \omega_2^1 \big) + Q_\theta \delta \varepsilon_4^0 + Q_x \delta \varepsilon_5^0 \Big] R dx d\theta \qquad (9)$$

$$I_i = \int\limits_{-h/2}^{h/2} \rho(z) \left(1 + \frac{z}{R} \right) (z)^i dz, \quad (i = 0,1,2)$$

where the dot superscript shows differentiation with respect to time. δW_{nc} is variation of the work done by non-conservative forces. Since, as known, follower forces are non-conservative, δW_{nc} for a cantilevered cylindrical shell can be written as [15]:

$$\delta w_{nc} = -\left[\int\limits_0^1 \left(\bar{P}'(x) \frac{\partial v}{\partial x} + \bar{P}(x) \frac{\partial^2 v}{\partial x^2} \right) dx \right] \delta v - \left[\int\limits_0^1 \left(\bar{P}'(x) \frac{\partial w}{\partial x} + \bar{P}(x) \frac{\partial^2 w}{\partial x^2} \right) dx \right] \delta w \qquad (10)$$

where $\bar{P} = P/2\pi R$ is the force per unit length of the shell circumference, on the premise that the axial stress is uniformly distributed along the thickness. Fig. 4 includes the scheme of Beck's follower loading.

Fig. 4 Schematic shape of follower loading in Beck's problem

In order to derive the equations of motion correctly, an additional constraint equation must be added to δU as follows [20]:

$$\iint \left(\frac{M_{\theta x}}{R} + N_{\theta x} - N_{x\theta} \right) \delta \varphi_n R dx d\theta \qquad (11)$$
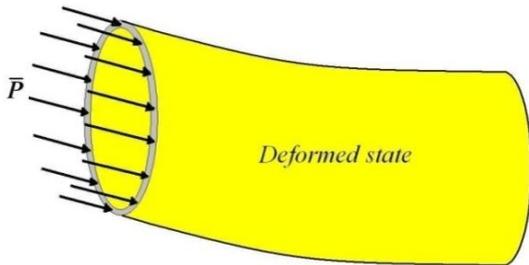
where $\delta \phi_n$ denotes the rotation about the transverse normal to the shell surface. For thin shells, $M_{x\theta} = M_{\theta x}, N_{x\theta} = N_{\theta x}$. Since the mode shapes used in the present research do not satisfy the natural boundary conditions, the boundary equations have been added to the domain equations. After replacing the stress resultants by their strain equivalents from Eq. (6) and replacing strain components in terms of deformations from Eq. (2), the following differential operators will be derived:

$$\int\limits_{t_1}^{t_2} \int\limits_0^{2\pi} \left(\int\limits_0^L [L]\{\Delta\} dx + \big[[L']\{\Delta\} \big]_0^L \right) R d\theta dt = \{0\}, \quad \{\Delta\} = \{u_0, v_0, w_0, \phi_x, \phi_\theta\}^T \qquad (12)$$

where L and L′ matrices are differential operators of the domain and boundary, respectively, whose elements are defined in Appendix A.

3. Solution Method

It can be proved that all of the equations are *orthogonal* in terms of θ if the displacements are defined using alternative sine and cosine functions as stated in Eq. (16). Thus, we can choose base functions and mode shape functions as follows:

$$u_0 = \sum_{j=1}^q U_j(x) \cos(n\theta) e^{\omega t}, \ U_j(x) = a_j^1 \varphi_j^1(x)$$

$$v_0 = \sum_{j=1}^q V_j(x) \sin(n\theta) e^{\omega t}, \ V_j(x) = a_j^2 \varphi_j^2(x)$$

$$w_0 = \sum_{j=1}^q W_j(x) \cos(n\theta) e^{\omega t}, \ W_j(x) = a_j^3 \varphi_j^3(x) \qquad (13)$$

$$\phi_x = \sum_{j=1}^q X_j(x) \cos(n\theta) e^{\omega t}, \ X_j(x) = a_j^4 \varphi_j^4(x)$$

$$\phi_\theta = \sum_{j=1}^q Y_j(x) \sin(n\theta) e^{\omega t}, \ Y_j(x) = a_j^5 \varphi_j^5(x)$$

The superscripts denote functions corresponding to u_0, ..., and ϕ_θ, and a_j^i ($i = 1..5$) are the unknown coefficients that could be determined by exerting any approximation method such as Galerkin's method. For the mode shape functions, $\varphi_j^i(x)$ ($i = 1..5$) that satisfy the essential boundary conditions of the cantilevered cylinder, the following polynomials have been taken [11, 24]:

$$\varphi_j^1 = \varphi_j^2 = x^j, \quad \varphi_j^3 = x^{j+1}, \quad \varphi_j^4 = \frac{d\varphi_j^3}{dx}, \quad \varphi_j^5 = \varphi_j^3 \quad (14)$$

After application of Galerkin's method, stiffness and mass matrices can be defined as functions of circumferential mode number, n, and power parameter, N. The stiffness matrix is also a function of $\bar{P}$. The equations obtained by the application of the so-called generalized Galerkin method are algebraic equations in terms of a_j^i ($i = 1..5$). Setting the determinant of the coefficient matrix to zero to impose the condition of non-trivial solution, as stated in Eq. (15), ω will be obtained.

$$\det\left(\boldsymbol{K}_{(\bar{P}, n, N)} + \omega^2 \boldsymbol{M}_{(n, N)}\right) = 0 \quad (15)$$

where ω is a complex number with a zero real part until the shell loses its stability under the applied follower forces. As soon as instability occurs, the real part begins to become positive or negative. In order to facilitate verification for future works, the non-dimensional load parameter β_s for the shell model can be considered as the comparator, defined as follows [14]:

$$\beta_s = \frac{1 - \nu^2}{Eh} \bar{P} \quad (16)$$

4. Results and Discussion

Calculations in the present study demonstrated the optimum number of terms needed for convergence in the Galerkin method is 6, which is confirmed in Ref. [11]. Subsection 4.1 includes verification of results with previous works. When the imaginary part of the natural frequency (ω) of two sequential modes becomes zero and the real part gets greater than zero, divergence occurs. Alternatively, when the imaginary part of the natural frequency of two sequential modes becomes equal and the real part gets greater than zero, flutter occurs. Results

demonstrated that instability under follower forces can be flutter or divergence. However, flutter always takes place before divergence.

4.1. Free Vibration of FGM shells

The minimum natural frequency (pertaining to the first mode) vs. the circumferential mode number for a stainless steel- nickel *FGM* shell with the following properties is shown in Fig. 5. In this case, the metal and ceramic phases have been taken to be stainless steel and nickel, respectively. The results were verified with those of Ref. [24].
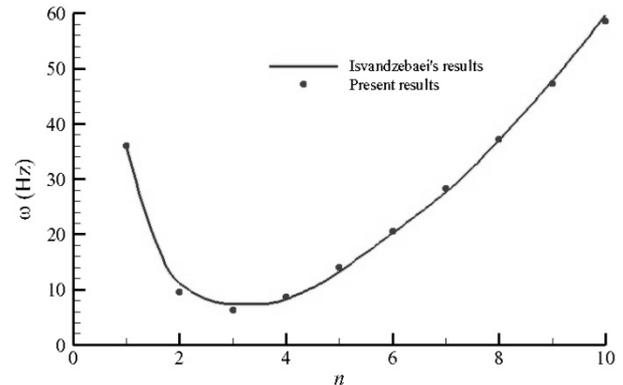

Fig. 5 Minimum natural frequency vs. the circumferential mode number for a cantilevered cylindrical *FGM* shell

4.2. Effect of axial deformation on flutter of cantilevered FGM cylindrical shells

The results in this section include the effect of axial deformation on the critical circumferential mode number and the critical (flutter) load. In order to evaluate the effects of elasticity modulus and power parameter in the case of considering axial deformation separately, the results have been calculated for homogeneous shells with different materials and for *FGM* materials of two constitutions: nickel-stainless steel and stainless steel-alumina.

4.2.1. Effect on the critical circumferential mode number

The effect of axial deformation on the critical circumferential mode number (n_{cr}) for homogeneous materials with different elasticity moduli is illustrated in Tables 3-5.

Table 3 Effect of axial deformation on n_{cr} for nickel (*Ni*)

h/R	$L/R = 10$		$L/R = 20$		$L/R = 40$		$L/R = 60$		$L/R = 80$		$L/R = 100$	
	$B^\dagger$	$C^{\dagger\dagger}$	B	C	B	C	B	C	B	C	B	C
0.01	5	5	4	4	3	3	3	3	2	2	2	2
0.03	3	3	3	3	2	2	2	2	2	2	2	2
0.05	3	3	2	2	2	2	2	2	2	2	1	1
0.075	3	3	2	2	2	2	1	1	1	1	1	1
0.1	2	2	2	2	2	2	1	1	1	1	1	1

h/R												
0.125	2	2	2	2	1	1	1	1	1	1	1	1
0.15	2	2	2	2	1	1	1	1	1	1	1	1
0.175	2	2	2	2	1	1	1	1	1	1	1	1
0.2	2	2	2	2	1	1	1	1	1	1	1	1

Table 4 Effect of axial deformation on n_{cr} for stainless steel (*Fe*)

h/R	$L/R = 10$		$L/R = 20$		$L/R = 40$		$L/R = 60$		$L/R = 80$		$L/R = 100$	
	B	C	B	C	B	C	B	C	B	C	B	C
0.01	5	5	4	4	3	3	3	3	2	2	2	2
0.03	3	3	3	3	2	2	2	2	2	2	2	1
0.05	3	3	2	2	2	2	2	2	2	2	1	1
0.075	3	3	2	2	2	2	2	2	1	1	1	1
0.1	2	2	2	2	2	2	1	1	1	1	1	1
0.125	2	2	2	2	1	1	1	1	1	1	1	1
0.15	2	2	2	2	1	1	1	1	1	1	1	1
0.175	2	2	2	2	1	1	1	1	1	1	1	1
0.2	2	2	2	2	1	1	1	1	1	1	1	1

Table 5 Effect of axial deformation on n_{cr} for alumina (*Al_2O_3*)

h/R	$L/R = 10$		$L/R = 20$		$L/R = 40$		$L/R = 60$		$L/R = 80$		$L/R = 100$	
	B	C	B	C	B	C	B	C	B	C	B	C
0.01	5	5	5	4	4	3	4	3	3	2	3	2
0.03	3	3	3	3	2	2	2	2	2	2	2	2
0.05	3	3	3	2	2	2	2	2	2	2	1	1
0.075	3	3	3	2	2	2	2	2	2	2	1	1
0.1	3	2	2	2	2	2	2	1	1	1	1	1
0.125	3	2	2	2	2	1	1	1	1	1	1	1
0.15	2	2	2	2	2	1	1	1	1	1	1	1
0.175	2	2	2	2	1	1	1	1	1	1	1	1
0.2	2	2	2	2	1	1	1	1	1	1	1	1

†: Beck's problem; *††*: Combined-effect problem (considering the axial deformation)

Moreover, the same effect on n_{cr} of nickel-stainless steel and stainless steel-alumina *FGM* materials with the power parameter *N=1* is included in Tables 6 and 7, respectively. The effect of axial deformation on n_{cr} for power parameters between 0 and 1 are like the corresponding effect for *N=0*, and the same effect for power parameters between 1 and ∞ are similar to the corresponding effect for *N=∞* (with very slight cases of difference occurring due to calculation errors). For this reason, n_{cr} values for intermediary power parameters have been disregarded for the sake of convenience.

It can be observed from Tables 3-7 that:

The combined-effect n_{cr} is, in all cases, less or equal to n_{cr} of ordinary Beck's problem. However, this effect does not influence n_{cr} remarkably.

The effect of considering axial deformation is the utmost in alumina and the least in nickel (in which n_{cr} does not change at all). Furthermore, the change in in *FGM* materials occurs between those in the two base phases. Thus, the so-called effect is proportional to the overall elasticity modulus of the cross section.

Table 6 Effect of axial deformation on n_{cr} for '*Ni-Fe*' *FGM* with *N=1*

h/R	$L/R = 10$		$L/R = 20$		$L/R = 40$		$L/R = 60$		$L/R = 80$		$L/R = 100$	
	B	C	B	C	B	C	B	C	B	C	B	C
0.01	5	5	4	4	3	3	3	3	2	2	2	2
0.03	3	3	3	3	2	2	2	2	2	2	2	2
0.05	3	3	2	2	2	2	2	2	2	2	2	2
0.075	2	2	2	2	2	2	2	2	1	1	1	1
0.1	2	2	2	2	2	2	1	1	1	1	1	1
0.125	2	2	2	2	1	1	1	1	1	1	1	1
0.15	2	2	2	2	1	1	1	1	1	1	1	1
0.175	2	2	2	2	1	1	1	1	1	1	1	1
0.2	2	2	1	1	1	1	1	1	1	1	1	1

Table 7. Effect of axial deformation on n_{cr} for '$Fe\text{-}Al_2O_3$' FGM with $N=1$

h/R	$L/R = 10$		$L/R = 20$		$L/R = 40$		$L/R = 60$		$L/R = 80$		$L/R = 100$	
	B	C	B	C	B	C	B	C	B	C	B	C
0.01	5	5	4	4	3	3	3	3	2	2	2	2
0.03	3	3	2	2	2	2	2	2	2	2	2	2
0.05	2	2	2	2	2	2	2	2	1	1	1	1
0.075	2	2	2	2	1	1	1	1	1	1	1	1
0.1	2	2	2	2	1	1	1	1	1	1	1	1
0.125	2	2	1	1	1	1	1	1	1	1	1	1
0.15	2	2	1	1	1	1	1	1	1	1	1	1
0.175	1	1	1	1	1	1	1	1	1	1	1	1
0.2	1	1	1	1	1	1	1	1	1	1	1	1

4.2.2. Effect on the flutter load

The effect of axial deformation on the non-dimensional flutter load (β_{scr}) for homogeneous materials with different elasticity moduli is illustrated in Tables 8-10, where η_C is the ratio of the combined-effect β_{scr} to the ordinary Beck's β_{scr}.

Table 8 Values of η_C due to the effect of axial deformation for nickel

$\dfrac{L}{h}$	10	20	40	60	80	100
0.01	1.19	1.20	1.20	1.18	1.18	1.18
0.03	1.22	1.19	1.19	1.19	1.18	1.17
0.05	1.18	1.19	1.20	1.17	1.16	1.15
0.075	1.18	1.21	1.17	1.16	1.17	1.17
0.1	1.23	1.19	1.17	1.17	1.17	1.17
0.125	1.19	1.19	1.17	1.17	1.17	1.17
0.15	1.18	1.19	1.17	1.17	1.17	1.17
0.175	1.19	1.19	1.17	1.17	1.17	1.17
0.2	1.19	1.19	1.17	1.17	1.17	1.17

Table 9 Values of η_C for stainless steel

$\dfrac{L}{h}$	10	20	40	60	80	100
0.01	1.24	1.24	1.23	1.23	1.17	1.18
0.03	1.25	1.22	1.22	1.22	1.22	1.22
0.05	1.22	1.22	1.22	1.20	1.18	1.17
0.075	1.22	1.24	1.20	1.17	1.17	1.17
0.1	1.23	1.23	1.19	1.17	1.17	1.17
0.125	1.25	1.21	1.17	1.17	1.17	1.17
0.15	1.22	1.21	1.17	1.17	1.17	1.17
0.175	1.21	1.21	1.17	1.17	1.17	1.17
0.2	1.21	1.21	1.17	1.17	1.17	1.17

Table 10 Values of η_C for alumina

$\dfrac{L}{h}$	10	20	40	60	80	100
0.01	1.16	1.19	1.21	1.25	1.28	1.24
0.03	1.19	1.19	1.19	1.19	1.16	1.15
0.05	1.19	1.49	1.78	1.78	1.76	1.55
0.075	1.50	1.78	1.78	1.76	1.76	1.17
0.1	1.71	1.80	1.78	1.19	1.17	1.17
0.125	1.65	1.80	1.55	1.17	1.17	1.17
0.15	1.70	1.80	1.19	1.17	1.17	1.17
0.175	1.79	1.81	1.17	1.17	1.17	1.17
0.2	1.79	1.82	1.17	1.17	1.17	1.17

Moreover, the same effect on β_{scr} of nickel-stainless steel and stainless steel-alumina *FGM* materials with $h/R = 0.1$ is shown in Figs 6 and 7, respectively. Diagrams for more intermediary power parameters have been disregarded for more clarity of figures.

As it can be seen in Tables 8-10 and Figs 6 and 7:
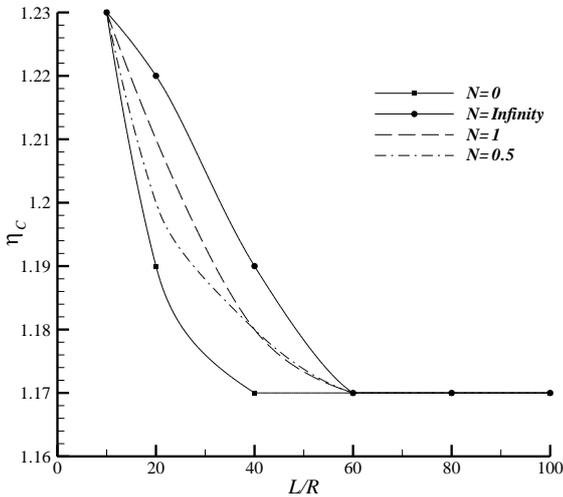
Fig. 6 Values of η_C for the nickel-stainless steel *FGM* with $h/R=0.1$
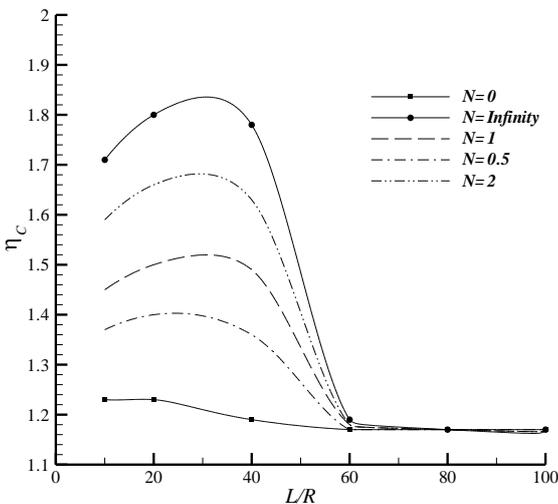
Fig. 7 Values of η_C for the stainless steel-alumina *FGM* with $h/R=0.1$

The axial deformation of the shell increases the flutter load to a limited extent. Namely, neglecting this effect overestimates the flutter load.

The axial deformation invariably reduces with *L/R* in *FGMs* where the elasticity moduli of the two phases are close, as for nickel-stainless steel. However, it has a maximum point in *FGMs* where the elasticity moduli of the two phases are far different, as for stainless steel-alumina. The maximum effect, i.e. the maximum value of η_C occurs in the range $20 < L/R < 40$, most probably in $L/R = 30$.

As the shell becomes very long and moderately thick, i.e. in beam-like ranges, η_C becomes almost constantly equal to 1.17 for all lengths and thicknesses.

The effect of axial deformation on the flutter load is proportional to the elasticity modulus of the whole cross section. Therefore, especially in thick, moderately-long shells, η_C is maximum in alumina, minimum in nickel, and approximately the average in both *FGM* shells with *N=1*.

It could be estimated from Figs 6 and 7 that η_C in an *FGM* shell can be approximately obtained with Eq. 4, whence η_C for a specific *N* is obtained by placing η_C instead of *F* and letting $z = 0$. Thus, it can be written that:

$$\eta_{Eff}\left(\eta_m, \eta_c, N\right) = \left(\eta_m - \eta_c\right)\left(\frac{1}{2}\right)^N + \eta_c, \quad \eta:\left(\eta_{LB}, \eta_{HB}\right) \quad (17)$$

For instance, the values of η_C, obtained from Eq. 4 and directly calculated from the program, are depicted in Fig. 8 for $N = 2$. Similar agreement was observed between the two methods for other power parameters. The zero and infinity power parameters are excluded because they refer to the very base phases made of different materials, and thus the values of η_C for these base phases have to be directly calculated. However, for a composite *FGM* consisting of the two base materials mixed according to the power mixture law, the same effect need not be calculated with discrete calculation.
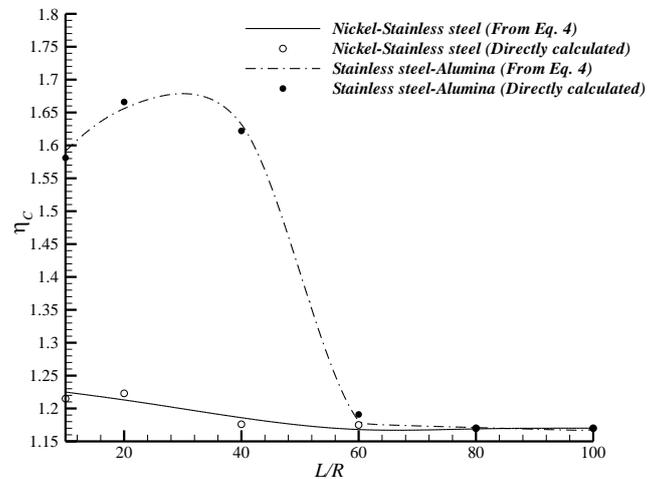
Fig. 8 Comparison between the values of η_C obtained using Eq. 17 and calculated directly for *FGM*s with *N=2*

5. Conclusions

The present study deals with the effect of considering the axial deformation of cantilevered cylindrical shells made of *FGM* materials on the dynamic instability, i.e. flutter under an axial follower force (Beck's loading).

First-order shear deformation was considered to derive differential equations, and Galerkin's method was applied using six longitudinal modes. Results included the effect of axial deformation (combined effect) on the critical circumferential mode number (n_{cr}) and non-dimensional flutter load (β_{scr}), which were deduced as follows:

- The combined-effect n_{cr} is less or equal to n_{cr} of ordinary Beck's problem.
- The axial deformation effect is proportional to the overall elasticity modulus of the cross section.
- The axial deformation of the shell increases the flutter load to a limited extent.
- The axial deformation effect is more significant in moderately-long, thick shells.
- In beam-like ranges, the combined-effect β_{scr} is almost constantly equal to 1.17 times the Beck's-loading β_{scr} for all lengths and thicknesses.

- The effect of axial deformation on the flutter load is proportional to the elasticity modulus of the whole cross section, both in homogeneous and *FGM* shells. For a power parameter other than zero and infinity, the effect of axial deformation can be obtained, without discrete computation, using the mixture formula of the *FGM*, knowing the corresponding values for the two phases.

Appendix A

$$L_{11} = A_{11}\frac{\partial^2}{\partial x^2} + \left(\frac{A_{66}}{R^2} - \frac{1}{2}\frac{B_{66}}{R^3}\right)\frac{\partial^2}{\partial\theta^2} - I_0\frac{\partial^2}{\partial t^2}, \quad L_{12} = \left(\frac{A_{12}+A_{66}}{R} - \frac{1}{2}\frac{B_{66}}{R^2}\right)\frac{\partial^2}{\partial x\partial\theta}$$

$$L_{13} = \frac{A_{12}}{R}\frac{\partial}{\partial x}, \quad L_{14} = B_{11}\frac{\partial^2}{\partial x^2} + \left(\frac{B_{66}}{R^2} - \frac{D_{66}}{R^3}\right)\frac{\partial^2}{\partial\theta^2} - I_1\frac{\partial^2}{\partial t^2}, \quad L_{15} = \left(\frac{B_{12}+B_{66}}{R} - \frac{1}{2}\frac{D_{66}}{R^2}\right)\frac{\partial^2}{\partial x\partial\theta}$$

$$L_{21} = \left(\frac{A_{12}+A_{66}}{R} + \frac{1}{2}\frac{B_{66}}{R^2}\right)\frac{\partial^2}{\partial x\partial\theta}, \quad L_{22} = -\bar{P}'(x)\frac{\partial}{\partial x} + \left(A_{66} + \frac{1}{2}\frac{B_{66}}{R} - \bar{P}(x)\right)\frac{\partial^2}{\partial x^2} + \frac{A_{22}}{R^2}\frac{\partial^2}{\partial\theta^2} - \frac{K_sA_{44}}{R^2} - I_0\frac{\partial^2}{\partial t^2},$$

$$L_{23} = \left(\frac{A_{22}}{R^2} + \frac{K_sA_{44}}{R^2}\right)\frac{\partial}{\partial\theta}, \quad L_{24} = \left(\frac{B_{12}+B_{66}}{R} + \frac{1}{2}\frac{D_{66}}{R^2}\right)\frac{\partial^2}{\partial x\partial\theta}, \quad L_{25} = \left(B_{66} + \frac{1}{2}\frac{D_{66}}{R}\right)\frac{\partial^2}{\partial x^2} + \frac{B_{22}}{R^2}\frac{\partial^2}{\partial\theta^2} + \frac{K_sA_{44}}{R} - I_1\frac{\partial^2}{\partial t^2}$$

$$L_{31} = -L_{13}, \quad L_{32} = -L_{23}, \quad L_{33} = -\bar{P}'(x)\frac{\partial}{\partial x} + \left(K_sA_{55} - \bar{P}(x)\right)\frac{\partial^2}{\partial x^2} - \frac{A_{22}}{R^2} + \frac{K_sA_{44}}{R^2}\frac{\partial^2}{\partial\theta^2} - I_0\frac{\partial^2}{\partial t^2}$$

$$L_{34} = \left(-\frac{B_{12}}{R} + K_sA_{55}\right)\frac{\partial}{\partial x}, \quad L_{35} = \left(-\frac{B_{22}}{R^2} + \frac{K_sA_{44}}{R}\right)\frac{\partial}{\partial\theta}$$

$$L_{41} = B_{11}\frac{\partial^2}{\partial x^2} + \frac{B_{66}}{R^2}\frac{\partial^2}{\partial\theta^2} - I_1\frac{\partial^2}{\partial t^2}, \quad L_{42} = \left(\frac{B_{12}+B_{66}}{R}\right)\frac{\partial^2}{\partial x\partial\theta}, \quad L_{43} = -L_{34}$$

$$L_{44} = -K_sA_{55} + D_{11}\frac{\partial^2}{\partial x^2} + \frac{D_{66}}{R^2}\frac{\partial^2}{\partial\theta^2} - I_2\frac{\partial^2}{\partial t^2}, \quad L_{45} = \left(\frac{D_{12}+D_{66}}{R}\right)\frac{\partial^2}{\partial x\partial\theta}$$

$$L_{51} = \left(\frac{B_{12}+B_{66}}{R}\right)\frac{\partial^2}{\partial x\partial\theta}, \quad L_{52} = B_{66}\frac{\partial^2}{\partial x^2} + \frac{B_{22}}{R^2}\frac{\partial^2}{\partial\theta^2} + \frac{K_sA_{44}}{R} - I_1\frac{\partial^2}{\partial t^2}, \quad L_{53} = -L_{35}$$

$$L_{54} = L_{45}, \quad L_{55} = -K_sA_{44} + D_{66}\frac{\partial^2}{\partial x^2} + \frac{D_{22}}{R^2}\frac{\partial^2}{\partial\theta^2} - I_2\frac{\partial^2}{\partial t^2}$$

$$L'_{11} = -A_{11}\frac{\partial}{\partial x}, \quad L'_{12} = -\frac{A_{12}}{R}\frac{\partial}{\partial\theta}, \quad L'_{13} = -\frac{A_{12}}{R}, \quad L'_{14} = -B_{11}\frac{\partial}{\partial x}, \quad L'_{15} = -\frac{B_{12}}{R}\frac{\partial}{\partial\theta}$$

$$L'_{21} = -\frac{A_{66}}{R}\frac{\partial}{\partial\theta}, \quad L'_{22} = A_{66}\frac{\partial}{\partial x}, \quad L'_{23} = 0, \quad L'_{24} = -\frac{B_{66}}{R}\frac{\partial}{\partial\theta}, \quad L'_{25} = -B_{66}\frac{\partial}{\partial x}$$

$$L'_{31} = L'_{32} = 0, \quad L'_{33} = -K_sA_{55}\frac{\partial}{\partial x}, \quad L'_{34} = -K_sA_{55}, \quad L'_{35} = 0$$

$$L'_{41} = L'_{14}, \quad L'_{42} = -\frac{B_{12}}{R}\frac{\partial}{\partial\theta}, \quad L'_{43} = -\frac{B_{12}}{R}, \quad L'_{44} = -D_{11}\frac{\partial}{\partial x}, \quad L'_{45} = -\frac{D_{12}}{R}\frac{\partial}{\partial\theta}$$

$$L'_{51} = -\frac{B_{66}}{R}\frac{\partial}{\partial\theta}, \quad L'_{52} = L'_{25}, \quad L'_{53} = 0, \quad L'_{54} = -\frac{D_{66}}{R}\frac{\partial}{\partial\theta}, \quad L'_{55} = -D_{66}\frac{\partial}{\partial x}$$

References

[1] Suresh S, Mortensen A. Fundamentals of Functionally Graded Materials, Maney Materials Science, the Institute of Materials, London, 1998, 165 p.

[2] Sofiyev AH. The stability of compositionally graded ceramic–metal cylindrical shells under aperiodic axial impulsive loading, Journal of Composite Structures, Elsevier, 2005, Vol. 69, pp. 247-257.

[3] Darabi M, Darvizeh M, Darvizeh A. Non-linear analysis of dynamic stability for functionally graded cylindrical shells under periodic axial loading, journal of Composite Structures, Elsevier, 2008, Vol. 83, pp. 201-211.

[4] Shariyat M. Dynamic thermal buckling of suddenly heated temperature-dependent fgm cylindrical shells, under combined axial compression and external pressure, International Journal of Solids and Structures, Elsevier, 2008, Vol. 45, pp. 2598-2612.

[5] Pellicano F. Dynamic stability and sensitivity to geometric imperfections of strongly compressed circular cylindrical shells under dynamic axial loads, Journal of Communications in Nonlinear Science and Numerical Simulation, 2009, Vol. 14, pp. 3449-3462.

[6] Huang Y, Li XF. Buckling of functionally graded circular columns including shear deformation, Journal of Materials and Design, Elsevier, 2010, Vol. 31, pp. 3159-3166.

[7] Sepiani HA, Rastgoo A, Ebrahimi F, Ghorbanpour Arani A. Vibration and buckling analysis of two-layered functionally graded cylindrical shell, considering the effects of transverse shear and rotary inertia, Journal of Materials and Design, Elsevier, 2010, Vol. 31, pp. 1063-1069.

[8] Alinia MM. A parametric investigation on stiffening axially loaded panels, International Journal of Civil Engineering (IJCE), 2004, No. 4, Vol. 2, pp. 246-256.

[9] Sabouri ghomi S, Kharazi MHK, Asghari A, Javidan P. Effect of stiffening rings on buckling stability of R. C. hyperbolic cooling towers, International Journal of Civil Engineering (IJCE), 2005, No. 1, Vol. 3, pp. 20-30.

[10] Rahai A, Alinia M, Salehi S. Cyclic performance of buckling restrained composite braces composed of selected materials, International Journal of Civil Engineering (IJCE), 2009, No. 1, Vol. 7, pp. 0-0.

[11] Simkins TE, Anderson GL. Stability of beck's column considering support characteristics, Journal of Sound and Vibration, Elsevier, 1975, No. 3, Vol. 39, pp. 359-369.

[12] Seyranian AP, Elishakoff I. Modern Problems of Structural Stability, International Centre for Mechanical Sciences, Springer-Verlag, Wien, New York, USA, 2002.

[13] Simitses J, Hodges DH. Fundamentals of Structural Stability, Butterworth-Heinemann Publications, Elsevier, USA, 2006, 389 p.

[14] Altman W, De Oliveira MG. Vibration Journal of and stability of cantilevered cylindrical shell panels under follower forces, Sound and Vibration, 1988, No. 2, Vol. 122, pp. 291-298.

[15] Altman W, De Oliveira MG. Vibration and stability of cantilevered cylindrical shell panels under follower forces, Journal of Sound and Vibration, 1990, No. 1, Vol. 136, pp. 45-50.

[16] Bismarck Nasr MN. Dynamic stability of shallow shells subjected to follower forces, AIAA Journal, 1995, No. 2, Vol. 33, pp. 355-360.

[17] Park SH, Kim JH. Dynamic stability of a completely free circular cylindrical shell subjected to a follower force, Journal of Sound and Vibration, 2000, No. 4, Vol. 231, pp. 989-1005.

[18] Torki ME, Kazemi MT. Effect of shell axial deformation on flutter of cantilevered cylindrical shells under follower forces, Journal of Computational and Applied Research in Mechanical Engineering (JCARME), 2012, No. 1, Vol. 2, pp. 15-24.

[19] Mahmoudkhani S, Haddadpour H, Navazi HM. Supersonic flutter prediction of functionally graded conical shells, Journal of Composite Structures, Elsevier, 2010, Vol. 92, pp. 377-386.

[20] Sohn KJ, Kim JH. Nonlinear thermal flutter of functionally graded panels under a supersonic flow, Journal of Composite Structures, Elsevier, 2009, Vol. 88, pp. 380-387.

[21] Haddadpour H, Navazi HM, Shadmehri F. Nonlinear oscillations of a fluttering functionally graded plate, Journal of Composite Structures, Elsevier, 2007, Vol. 79, pp. 242-250.

[22] Haddadpour H, Mahmoudkhani S, Navazi HM. Supersonic flutter prediction of functionally graded cylindrical shells, Journal of Composite Structures, 2008, Vol. 83, pp. 391-398.

[23] Reddy JN. Mechanics of Laminated Composite Plates and Shells, CRC press, Florida, USA, 2004, 782 p.

[24] Shen HS. Functionally-Graded Materials, Nonlinear Analysis of Plates and Shells, CRC press, USA, 2009, 280 p.

[25] Reddy JN, Chin CD. thermomechanical analysis of functionally graded cylinders and plates, Journal of Thermal Stresses, 1998, Vol. 21, pp. 593-626.

[26] Wu TL, Shukla KK, Huang JH. Nonlinear static and dynamic analysis of functionally graded plates, International Journal of Applied Mechanics and Engineering, 2006, Vol. 3, pp. 679-698.

[27] Isvandzibaei MR, Alinaghizadeh MR, Zaman AH. Vibration of functionally graded cylindrical shells under effect clamped-free boundary conditions using hamilton's principle, World Academy of Science, Engineering and Technology, 2010, Vol. 63, pp. 388-393.